Symmetrical Coupling Multi-Cavity Bandpass Filter for CMOS Compatible Fluorescence Detection

Wenbing Li and Chao Ping Chen

***Abstract*—Integration of functional components such as excitation light source, micro-fluidic chip, optical filters, and complementary metal–oxide–semiconductor (CMOS) sensors on a single photonics chip for fluorescence detection by advanced semiconductor process, is a future technology for rapid responding, high accuracy, and handheld point-of-care diagnosis protocol in field application of daily life. We designed a CMOS compatible bandpass filter on a glass substrate based on symmetrical coupling multi-cavity (SCMC) SiN/SiO_2 thin film stacker aimed at detection of 5-carboxylfluorescein (5-FAM), a commonly used fluorescence probe in biotechnology and medicine diagnosis. The calculation based on transfer matrix method (TMM) and 2D finite difference time domain (FDTD) algorithm, revealed that there was an optimized number of cavities in the SCMC stacker, for the transmittance in the pass band decreasing with the increment of the number of cavities while the optical density in the stop band improving with it. For a SCMC stacker with 10 resonant cavities, both the TMM and 2D FDTD calculation, figured out that the fluorescence emission and the remained excitation source should be directed to incident on the SCMC stacker with an angle less than 18° for a good passing of fluorescence emission centered at 520 nm and blocking of excitation light of a wavelength of 488 nm. It provided new insights for future design and fabrication of micro-lens array and micro-apertures array for the highly integrated photonics chip aimed at detection of fluorescence on a single chip.**

***Index Terms*—Finite difference time domain, fluorescence detection on chip, integrated photonics chip, symmetric coupling multi-cavities bandpass optical filter, transfer matrix method.**

I. Introduction

DETECTION of fluorescence with a configuration consisted of excitation light source, micro-fluidic chip, optical filters, and complementary metal–oxide–semiconductor (CMOS) sensors, plays a key role in the quantitative analysis of nucleic acid by polymerase chain reaction (PCR) [1], [2], [3], [4], [5], [6], [7]. In this special era that the COVID-19 has been threatening public health all over the world for almost 3 years since the end of year 2019, a rapid responding, portable, and high accuracy point-of-care diagnosis solution as PCR protocol, is in urgent demanding obviously. Optical filter made by all-dielectric thin film stacker, that compatible with the CMOS semiconductor process, is the promising solution for wafer scale integration of excitation laser source, optical filters, micro-fluidic chips, and CMOS sensors together to reduce the total volume of the PCR system, and enable high accuracy fluorescence detection possible on a highly integrated photonics chip.

Up to date, a lot of optical filters based on various design methods, are available in literatures [8], [9], [10], [11], [12], [13], [14], [15], [16], [17], [18]. On the early days, Baumeister described a method to design a band pass optical filter that combined of an antireflection stacker on the surface, an antireflection stacker on a transparent substrate, and a core equivalent stacker sandwiched between the two antireflection stackers [19]. In case the phase thickness of the core equivalent stacker was pure real, there was a pass band existed in the transmission spectrum, otherwise, the stop band appeared [19]. Macleod reviewed methods to design a bandpass optical filter that composed of a short pass optical filter at long wavelength and a long pass optical filter at short wavelength deposited at each side of a transparent substrate [20]. After reviewing Thelen's technique for designing optical filters, Macleod pointed out a multiple cavities optical filter that contained several core periods such as *mA BABABA mA,* and an antireflection stacker on its surface, was promising for a flat pass band without "Rabbit ears" and high optical density stop bands to block the unwanted wavelengths [20]. With the support of high resolution lithography technique, the strip gratings was introduced to design and fabricate narrow band optical filter with a single resonant cavity [12], [21]. Furthermore, multiple layers of dielectric thin film alternated by multiple layers of strip gratings, promised a multiple resonant cavities band pass optical filter with high optical density [11], [14]. Besides the vertical optical filters, similar methods for designing optical filter horizontal to the surface of a substrate based on the one-dimensional photonic crystal, was illustrated in [9], [10]. With the assistance of computational electromagnetics, a bandpass optical filter based on two-dimensional photonic crystals was designed by Robinson et al. [22], which was possible for using the photonics integrated circuits (PIC) for optical communications application.

The transfer matrix method (TMM) was the most popular theory for design of thin film optical filters, for its high accuracy and easiness for calculation [20]. As an analogy to the RF filter [23], the scattering matrix method was also usually used to design the optical filters [11], [14]. In this article, we proposed a CMOS compatible bandpass optical filter, consisted

Manuscript received 23 November 2022; accepted 29 November 2022. Date of current version 8 December 2022. This work was supported in part by the National Natural Science Foundation of China under Grants 61901264 and 61831015, in part by the Science and Technology Commission of Shanghai Municipality under Grant 19ZR1427200, and in part by the Natural Science Foundation of Chongqing under Grant cstc2021jcyj-msxmX1136. *(Corresponding author: Chao Ping Chen.)*

Wenbing Li is with the Shanghai Industrial μTechnology Research Institute, Shanghai 201899, China (e-mail: quentinlee08@foxmail.com).

Chao Ping Chen is with the Smart Display Lab, Department of Electronic Engineering, Shanghai Jiao Tong University, Shanghai 200240, China (e-mail: ccp@sjtu.edu.cn).

Digital Object Identifier 10.1109/JPHOT.2022.3226568

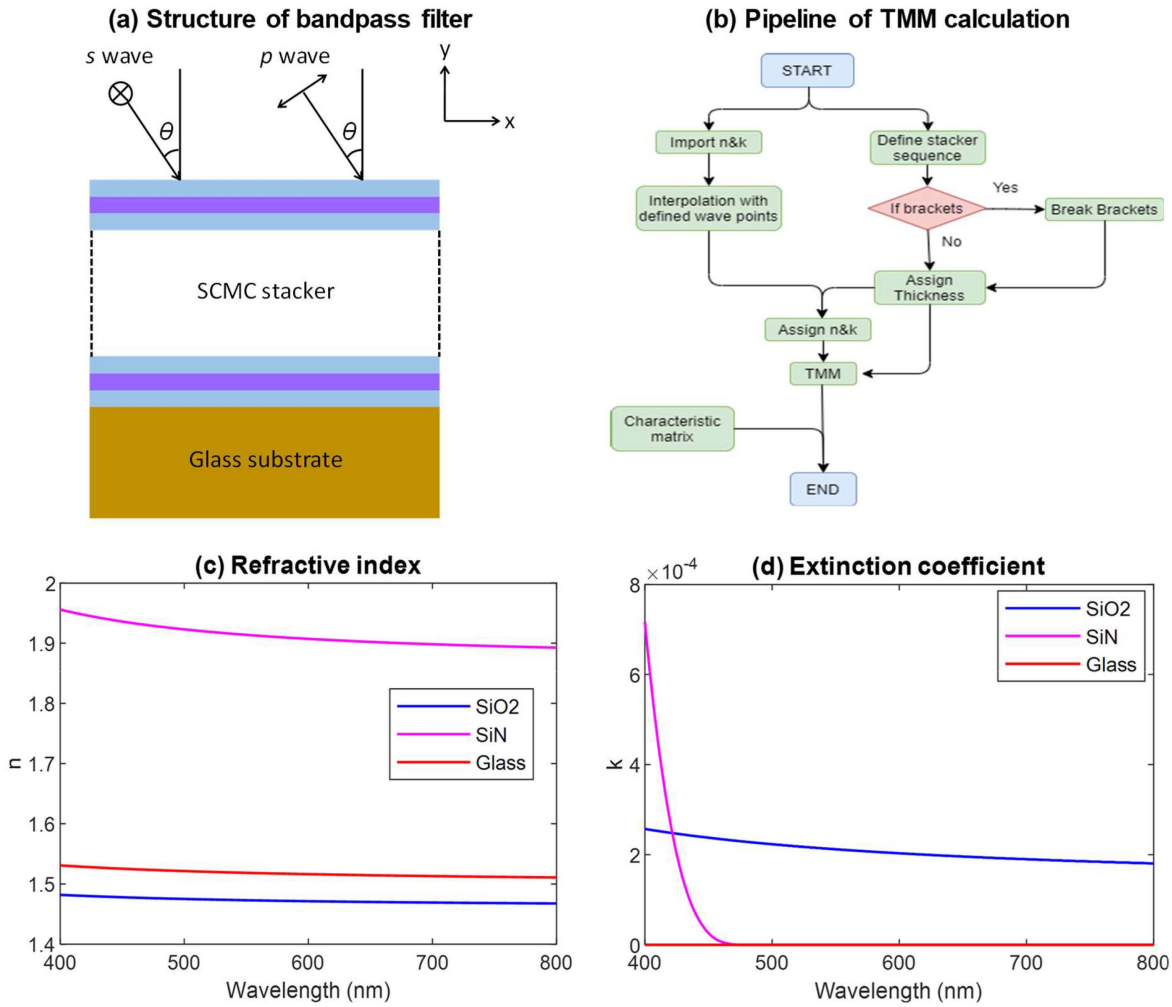

Fig. 1. (a) Schematic of the band pass optical filter combined of SiN/SiO_2 multiple layers stacker on a glass substrate, p/s polarized light wave incident on the surface of the stacker with an angle θ; (b) pipeline of the calculation based on TMM theory; (c) refractive index; and (d) extinction coefficient for SiN, SiO_2, and glass substrate.

of a symmetrical sequence of multiple resonant cavities made by SiN/SiO_2 alternative stacker. The low refractive index SiO_2 was used as the material of the half wavelength cavity, which was sandwiched between two reflectors combined of quarter wavelength alternating SiN/SiO_2 stacker. It was a simple all dielectric Fabry-Perot cavity and was used as a unit to compose the bandpass optical filter. A quarter wavelength SiO_2 was used as the spacer to separate each Fabry-Perot cavity. Replacing of the anti-reflection stacker on the top surface and the substrate, the same Fabry-Perot cavities with low reflection reflectors were used instead. The TMM algorithm was used to calculate the transmission spectrum and optical density depends on the number of resonant cavities and the angle of incidence, respectively. For a comparative study, the 2D finite difference time domain (FDTD) method was also implemented to calculate the transmission spectrum and optical density at wavelength scale. For a detail study of the waves in the symmetrical coupling multi-cavity (SCMC) stack, the electric field and magnetic field at each layer for the p/s polarized incident plane wave, were also calculated respectively. The power oscillation in each cavity was also given out with a vertical incidence and an angle of incidence respectively. Our research provides a new insight for future CMOS compatible bandpass optical filter design and fabrication for highly integrated lab-on-chips used in fluorescence detection and point-of-care diagnosis.

II. Design and Method

As showed in the schematic in Fig. 1(a), we designed a SCMC bandpass optical filter based on SiN (H: high index quarter wavelength layer) and SiO_2 (L: low index quarter wavelength layer) thin films stacker on a glass substrate (The refractive index of SiN, SiO_2 and glass substrate showed in Fig. 1(c) and (d)), which can be expressed as the following sequence: $Air / (HL)^2\ H2LH\ (LH)^2L\ [(HL)^3H2LH\ (LH)^3L]^{m-2}(HL)^2H2LH\ (LH)^2/Glass$, where m is the total number of optical cavities in the stacker.

The core periods of the bandpass optical filter was a number of repeated Fabry-Perot cavities: $(HL)^3H2LH\ (LH)^3$, separated by a spacer layer "L". It was sandwiched between two other Fabry-Perot cavities with fewer reflector layers: $(HL)^2\ H2LH\ (LH)^2$. In order to enable the emission of the fluorescence

passing through the SCMC stacker and blocking the excitation wavelength with a high optical density, the thickness of H and L layer was determined by a quarter wavelength that close to the emission peak and the refractive index of related thin film. The thickness of H and L layer could be tuned to match the requirement of various fluorescence with different excitation wavelength and emission wavelength. For the application in detection of 5-carboxylfluorescein (5-FAM) [24], [25], which had an emission peak about 518 nm and a unsymmetrical emission spectrum (referred to the emission peak) covered a broad wavelength range (518 to 700 nm) beyond the emission peak, a laser diode with a lasing wavelength at 488 nm based on GaN/InGaN quantum wells was selected as the light source. A center wavelength at 520 nm was selected to determine the thickness of H and L layer (H: 67.4 nm, L: 88 nm).

According to the transfer matrix method, the transmittance of the bandpass optical filter can be obtained by the surface optical admittance that calculated by multiplication of the characteristic matrix that represented each layer [20]. For a flexible calculation of multilayer stacker with arbitrary sequence, we compiled a script to read the sequence of the stacker, and to assign the thickness values and dispersive refractive index to each layer smartly while calculating the characteristic matrix (pipeline of TMM is given in Fig. 1(b)). The complex sequence of a multi-layer stacker combined of high and low index quarter wavelength layers with different repeated periodicities, which needs to use multiple brackets to include a sub-periodicity, is easy to be understood by the computer for assigning of refractive index *n*, extinction coefficient *k* and thickness values with our script. Therefore, it becomes quite simple to investigate how the transmittance and optical density values vary with the number of cavities. The *p* and *s* polarized light with an angle of incidence is distinguished by the tilted optical admittance [20].

For a detail study of the SCMC bandpass optical filter, we introduced the time resolved 2D FDTD method to calculate the transmittance and optical density in wavelength scale within a Cartesian coordinate system (Fig. 1(a)). In a 2D space based on Cartesian coordinate, the leap-frog equations for the FDTD algorithm can be expressed as followed with incidence of a linearly *p*-polarized plane wave [26]

$$\mathrm{H}_{\mathrm{z}\,\mathrm{i+1/2,\,j+1/2}}^{\mathrm{n+1/2}} = \mathrm{H}_{\mathrm{z}\,\mathrm{i+1/2,j+1/2}}^{\mathrm{n-1/2}} + \frac{\Delta \mathrm{t}}{\mu_{\mathrm{i+1/2,j+1/2}}} \times \left[\frac{\mathrm{E}_{\mathrm{x}\,\mathrm{i+1/2,j+1}}^{\mathrm{n}} - \mathrm{E}_{\mathrm{x}\,\mathrm{i+1/2,j}}^{\mathrm{n}}}{\Delta \mathrm{y}} - \frac{\mathrm{E}_{\mathrm{y}\,\mathrm{i+1,j+1/2}}^{\mathrm{n}} - \mathrm{E}_{\mathrm{y}\,\mathrm{i,j+1/2}}^{\mathrm{n}}}{\Delta \mathrm{x}} \right] \tag{1}$$

$$E_{x\,i+1/2,j}^{n+1} = E_{x\,i+1/2,j}^{n} + \frac{\Delta t}{\varepsilon_{i+1/2,j}\Delta y} \times \left[H_{z\,i+1/2,j+1/2}^{n+1/2} - H_{z\,i+1/2,j-1/2}^{n+1/2} \right] \tag{2}$$

$$E_{y\,i,j+1/2}^{n+1} = E_{y\,i,j+1/2}^{n} - \frac{\Delta t}{\varepsilon_{i,j+1/2}\Delta x} \times \left[H_{z\,i+1/2,j+1/2}^{n+1/2} - H_{z\,i-1/2,j+1/2}^{n+1/2} \right] \tag{3}$$

Only the time and space dependent field Hz, Ex, and Ey exist in this case. By contrast, with the incidence of a *s*-polarized linear source, only the Ez, Hx, Hy components exist, and the discrete leap-frog update equation in Yee grids can be expressed as follows [5]

$$H_{x\,i,j+1/2}^{n+1/2} = H_{x\,i,j+1/2}^{n-1/2} - \frac{\Delta t}{\mu_{i,j+1/2}} \left[E_{z\,i,j+1}^{n} - E_{z\,i,j}^{n} \right] \tag{4}$$

$$H_{y\,i+1/2,j}^{n+1/2} = H_{y\,i+1/2,j}^{n-1/2} + \frac{\Delta t}{\mu_{i+1/2,j}\Delta x} \left[E_{z\,i+1,j}^{n} - E_{z\,i,j}^{n} \right] \tag{5}$$

$$E_{z\,i,j}^{n+1} = E_{z\,i,j}^{n} + \frac{\Delta t}{\varepsilon_{i,j}} \times \left[\frac{H_{y\,i+1/2}^{n+1/2} - H_{y\,i-1/2,j}^{n+1/2}}{\Delta x} - \frac{H_{x\,i,j+1/2}^{n+1/2} - H_{x\,i,j-1/2}^{n+1/2}}{\Delta y} \right] \tag{6}$$

The frequency dependent electric field and magnetic field can be obtained from the time resolved field in FDTD algorithm through a Fourier transformation over the time steps in the time evolution [27].

$$F(\omega) = \int_{-\infty}^{+\infty} f(t)\, e^{-i\omega t} dt = \sum_{k=0}^{k=N} f(k\Delta t)\, e^{-i\omega k\Delta t} \Delta t \tag{7}$$

Therefore, the reflectance of the multiple thin film stacker can be calculated as the ratio between line integral of the power flow up at the back of the linear polarized plane wave over the injected power of the light source for a 2D simulation. Similarly, the transmittance of the multiple thin film stackers on a transparent substrate with little absorption can be calculated as the ratio between the line integral of the power flow down through the interface between bottom thin film and substrate, over the injected power of the light source. The expression for calculating the transmittance on a surface based on 3D FDTD method is expressed followed [27]

$$T = \frac{\frac{1}{2} \iint \vec{P}(x, y, z, \omega)\, d\vec{S}}{P(\omega)} \tag{8}$$

In case the simulation is in a 2D Cartesian system, the area integral of the power transmitted a surface became a line integral of the power passed through a line. Sequentially, the optical density of the multiple thin film layers stacker that evaluates how the stacker can block the light waves at specific wavelength, can be calculated as [20]

$$OD = \log T \tag{9}$$

The termination of the leap-frog update equations, namely, the shut-off value is determined by a value that defined by the ratio between the remained power in the simulation region and the injected source power. This value together with the size of Yee grids in simulation space and time steps in the time evolution, play a key role to obtain an accurate frequency dependent field from Fourier transformation of the time dependent field value. To limit the accuracy influence from Yee grids, we chose a

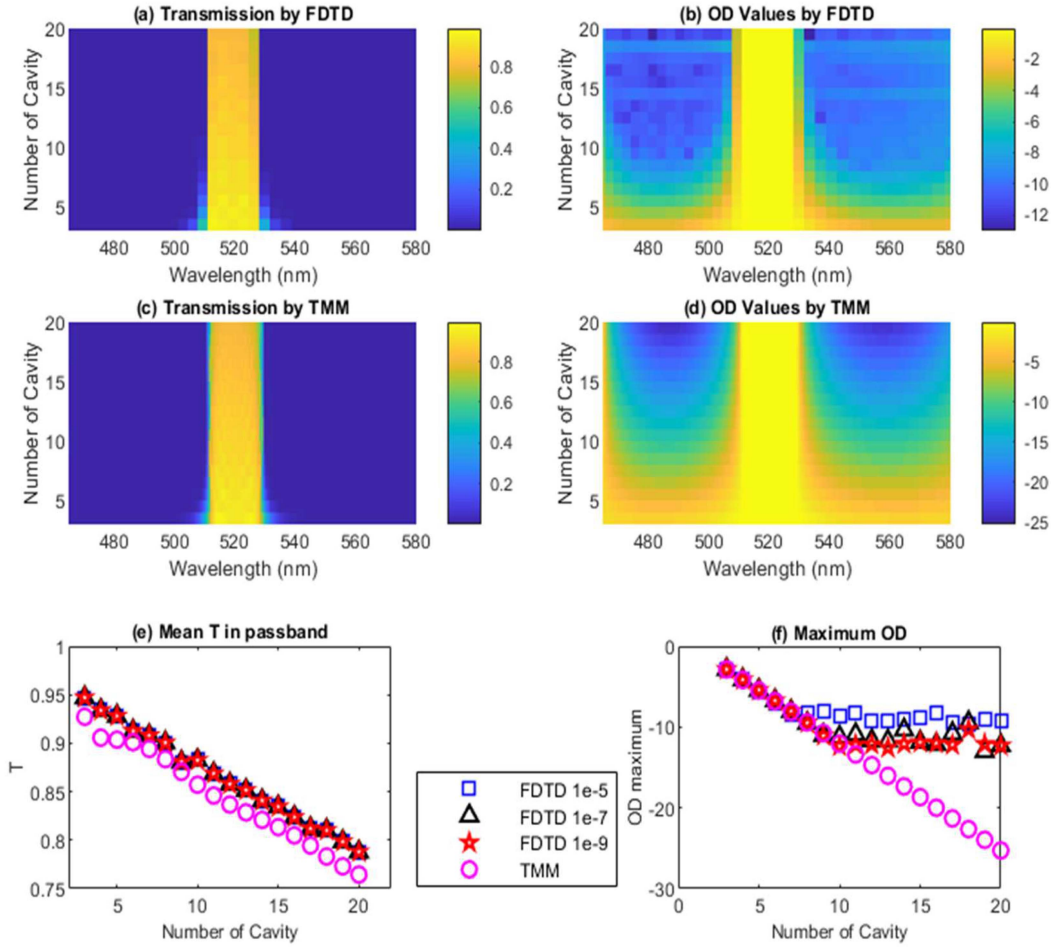

Fig. 2. Transmission and OD values of the *Air / (HL)^2 H2LH (LH)^{2}L [(HL)^{3}H2LH (LH)^{3}L]$^{m-2}$(HL)^{2}H2LH (LH)^2/Glass* band pass optical filter dependent on wavelength and number of cavities. The incident light was vertical to the surface of the optical filter. (a) Transmission of the band pass optical filter dependent on wavelength and number of cavities by FDTD method with a shut-off value as 1×10^{-7}. (b) OD values of the band pass optical filter dependent on wavelength and number of cavities by FDTD method with a shut-off value as 1×10^{-7}. (c) Transmission of the band pass optical filter dependent on wavelength and number of cavities by TMM. (d) OD values of the band pass optical filter dependent on wavelength and number of cavities by TMM. (e) Mean values of transmission in the pass band dependent on number of cavities, by FDTD with various shut-off values (1×10^{-5}, 1×10^{-7}, and 1×10^{-9}) and by TMM algorithm, respectively. (f) Maximum OD values dependent on number of cavities, by FDTD with various shut-off values (1×10^{-5}, 1×10^{-7}, and 1×10^{-9}) and by TMM algorithm, respectively.

grid size as small as 1/22 of the center wavelength for all the optical density calculation based on 2D FDTD. We performed the calculation of the transmission and optical density for the SCMC bandpass optical filter dependent on the number of resonant cavities, with various shut-off values such as 1×10^{-5}, 1×10^{-7}, and 1×10^{-9}, to investigate its influences for the computation accuracy compared with related results obtained from TMM algorithm.

III. Results and Discussion

The comparison of the transmission and optical density results from TMM algorithm and 2D FDTD method was shown in Figs. 2 and 3, dependent on the number of resonant cavities and angle of incidence respectively. The electric field, magnetic field, and power distribution in the SCMC thin films stacker at wavelength of 520 nm, with a vertical incidence was presented in Fig. 4. The power distribution in each resonant cavity of the SCMC stacker at wavelength of 474 nm and 469 nm, with an incidence of 45° for *p*/*s* linearly polarized waves respectively, was displayed in Fig. 5.

As presented in Fig. 2(a), the transmission band of the SCMC optical filter by 2D FDTD algorithm (with a shut-off value of 1×10^{-7}), showed a pass band among 511 nm to 528 nm, with different number of cavities in the SCMC stacker. Something worth to mention was that the s linearly polarized light source with a vertical incidence on the surface of the SCMC stacker was selected for both the TMM calculation and 2D FDTD algorithm, that only the Ez field and Hx field were existed (E = (0, 0, Ez), H = (Hx, 0, 0)). The selection of p or s linearly polarized wave for the computation with a vertical incidence source, did not make any difference since the electric field and magnetic field of the light wave propagating toward the SCMC stacker was axis symmetric referred to light injection axis in the x-y Cartesian coordinate system. The wideness of the pass band presented little change, while increasing the number of cavities. However, both the edge at short wavelength and the edge at long wavelength became steeper, with the increased

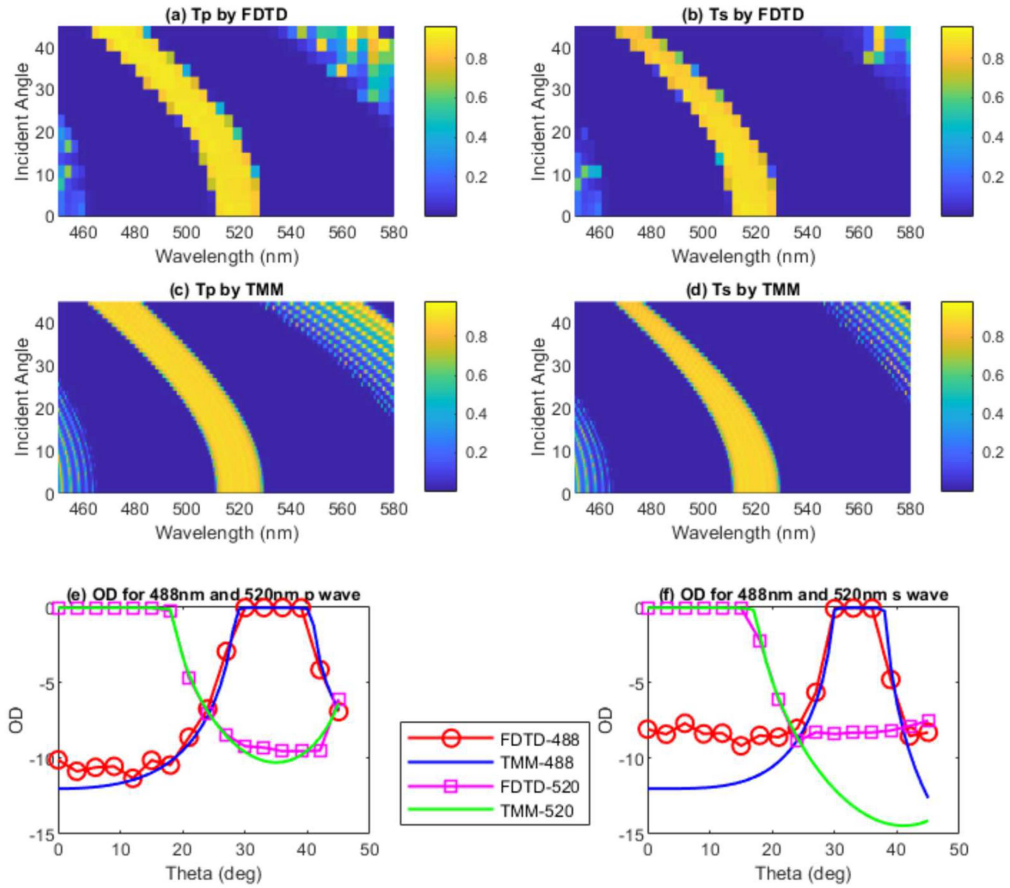

Fig. 3. Pass band of the optical filter *Air / (HL)^2 H2LH (LH)^{2}L [(HL)^{3}H2LH (LH)^{3}L]^8(HL)^{2}H2LH (LH)^2/Glass,* dependent on incident angle for p/s polarization light source. Transmission values dependent on incident angle for (a) *p*-polarized and (b) *s*-polarized light source, calculated by FDTD method. The shut-off value was 1×10^{-7} and 1×10^{-5} for the linearly p and s polarized wave, respectively, for all the simulations at various incident angle from 0° to 45°. Transmission values dependent on incident angle for (c) p and (d) s polarized light source, calculated by TMM algorithm. OD values dependent on incident angle, for (e) *p* and (f) *s* polarized light source with a wavelength at 488 and 520 nm, respectively.

number of the optical cavities. The optical density values from Fig. 2(b) at the stop region beyond 511 nm and 528 nm, increased with the increment of the number of resonant cavities. Similar results were obtained with the TMM calculation as presented in Fig. 2(c) and (d), except higher maximum optical density values were gotten for TMM calculation as the color scale showed in Fig. 2(d). For comparisons, the average transmittance of the pass band between 511 nm and 528 nm dependent on the number of resonant cavities, for the TMM calculation and the 2D FDTD calculation with various shut-off values (1×10^{-5}, 1×10^{-7}, and 1×10^{-9}), was displayed in Fig. 2(e) respectively. The average transmittance value was reduced linearly with increment of the number of cavities, from a value above 90% (TMM: 92.73%, 2D FDTD: 94.613%) with 3 resonant cavities to a value between 75% and 80% (TMM: 76.449%, 2D FDTD: 78.796%) with 20 resonant cavities. The data from TMM calculation and 2D FDTD algorithm matched with each other quite well, though the mean transmittance values for 2D FDTD algorithm showed a little bit larger than that of the TMM calculation. The slight contrast was possible from the number of frequency points used in the calculation, in which 1000 frequency points for TMM calculation among a wavelength range between 400 nm and 800 nm was included in the computation while only 100 frequency points among the same wavelength range was included in the computation by 2D FDTD algorithm for saving of RAM. Therefore, rather than the TMM calculation, a smaller number of frequency points in the pass band region were included in the computation of the average transmittance for the 2D FDTD algorithm. Furthermore, the mean transmittance values among the pass band region for different shut-off values (1×10^{-5}, 1×10^{-7}, and 1×10^{-9}) in the 2D FDTD computation, matched perfectly with each other at various number of resonant cavities from 3 to 20 in the scale shown in Fig. 2(e). The maximum optical density value among the wavelength range between 400 nm and 800 nm dependent on the number of resonant cavities in the SCMC stacker, was shown in Fig. 2(f) respectively for the TMM calculation and 2D FDTD with various shut-off values. It was obvious that the maximum optical density value computed by TMM calculation improved linearly with the increment of the number of cavities from -2.8808 (m $= 3$) to -25.2816 (m $= 20$). In case m was less than 7, the maximum optical density values calculated by the 2D FDTD algorithm matched well with that computed by TMM calculation. The optical density value improved almost linearly from -2.8808 with $m = 3$, to -8.1103 with $m = 7$. For a shut-off value as 1×10^{-5} for the 2D FDTD simulation, the optical density value

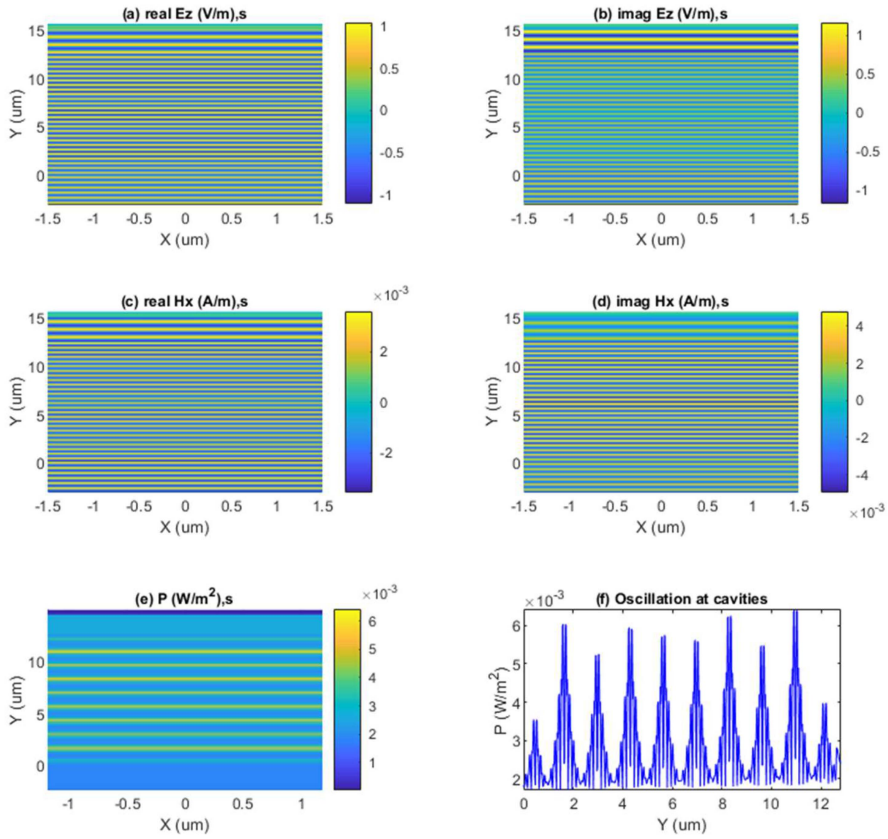

Fig. 4. Ez, Hx field, and power distribution in the optical filter *Air / (HL)^2 H2LH (LH)^{2}L [(HL)^{3}H2LH (LH)^{3}L]^8(HL)^{2}H2LH (LH)^2/Glass,* with vertical incidence of a s polarized plane wave. (a) Real part and (b) imaginary part of the Ez field respectively at 520 nm in the pass band. (c) Real part and (d) imaginary part of the Hx field respectively at 520 nm in the pass band. (e) top-view and (f) cross-section power oscillation at each cavity of the optical filter at 520 nm in the pass band.

did not improve further with the increasing of number of cavities and almost kept as constant around -8.11 for the number of cavities between 7 and 20. The same situation happened for the shut-off value as 1×10^{-7} and 1×10^{-9} for the 2D FDTD simulation, in which the optical density value started to deviate from that computed by TMM calculation when the number of cavities increased to 9 (with optical density value as -10.7467) and 10 (with a maximum optical density as -12.0674). The deviation of the optical density value by 2D FDTD from that by TMM, was originated from the termination condition of numerical iteration of the leap-frog equations in time evolution. A smaller shut-off value resulted in longer time propagation of light waves in the simulation region and more time steps involved in the calculation, which led to a longer time as the up limit for an integral from time dependent field to frequency dependent field in the Fourier transformation from time domain to frequency domain.

To investigate how the angle of incidence influences the pass band, we calculated the transmittance values of a SCMC stacker with $m = 10$ with a series of incident angles from 0 to 45° for p and s linearly polarized wave respectively. The calculation result obtained from 2D FDTD algorithm was presented in Fig. 3(a) and (b), while the data gotten from TMM calculation was shown in Fig. 3(c) and (d). The result presented that the center of the pass band blue shifted with the increasing of the incident angle for both the p and s polarized wave. For the p polarized wave, the center wavelength shifted to 474 nm from 520 nm, while for the s polarized wave, the center wavelength shifted to 469 nm from 520 nm. It was evident that the wideness of the pass band became narrower with the increasing of the incident angle for s polarized wave. To investigate how the SCMC band pass optical filter enables the FAM fluorescence emission at about 520 nm passing through while blocking the excitation laser diode lasing at 488 nm, the optical density value for light wave at 488 nm and 520 nm dependent on various incident angle from 0 to 45° for p/s polarized wave respectively, was displayed in Fig. 3(e) and (f). Both the 2D FDTD calculation and TMM calculation from Fig. 3(e), showed that the SCMC band pass optical filter blocked the 488 nm wave quite well for the *p*-polarized wave (with an OD value larger than -10), if the angle of incidence was less than 18°. However, with the increasing of the incident angle to 30°, the 488 nm wave started to pass through the SCMC band pass optical filter while the emission wave 520 nm began to be blocked. Similar result was observed from Fig. 3(f) for the s-polarized wave. The result from Fig. 3 suggested that the incident angle of the excitation source should be less than 18° for this SCMC stacker to enable the fluorescence emission passing through with a good blocking of the excitation wave. In a macro optical system, multiple optical components such as lens and apertures could be selected to satisfy the design target in a big sealed-in volume. For an integrated photonics chip that composed of functional devices such as laser source, lab-on-chip, optical filters, and CMOS sensors in a compact space, each layer-out should be designed smartly to satisfy both

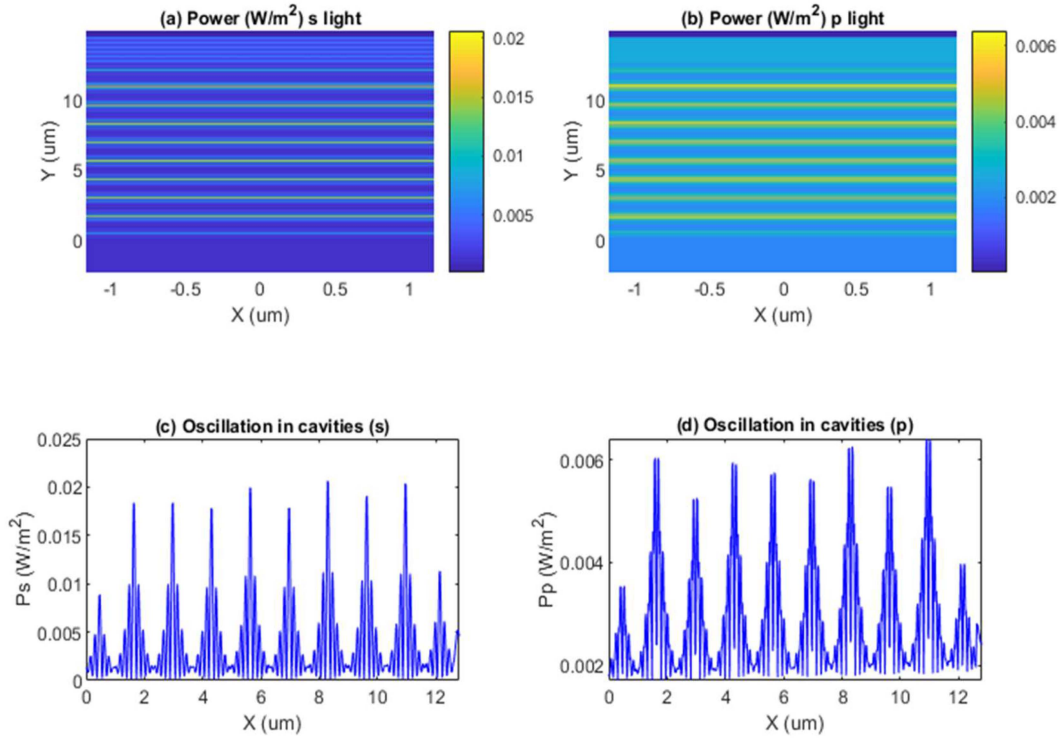

Fig. 5. Power oscillation in each cavity of the bandpass optical filter *Air / (HL)^2 H2LH (LH)^{2}L [(HL)^{3}H2LH (LH)^{3}L]^8(HL)^{2}H2LH (LH)^2/Glass*, with a *s/p* polarized source of a 45° incident angle respectively. Power in each cavity for (a) *s* and (b) *p* polarized source at 469 nm in the pass band. Oscillation in each cavity for (c) *s* and (d) *p* polarized source at 474 nm in the pass band.

of the functional requirement and semiconductor process compatibility. Therefore, microlens array with suitable focus length and micro-apertures with matched openings should be designed above the SCMC stacker to direct the excitation source and fluorescence emission propagating to the SCMC stacker with a small incident angle within 18°, and to focus the fluorescence emission at the active region of CMOS sensors with specified focus depth. That is our future work for the chip design.

The electric field Ez, magnetic field Hx, and power distribution in the SCMC stacker with $m = 10$ with a vertical incident plane wave of a wavelength as 520 nm, was displayed in Fig. 4. For this wavelength, the plane wave was observed transmitting through the SCMC stacker obviously with a high transmittance close to 90%. It was evident that the plane wave propagating downward with different transportation constant in the air above the SCMC stacker, in the thin film layers of the SCMC stacker, and in the glass substrate from the real and imagery part of Ez and Hx respectively from Fig. 4(a) to (d). The power distribution in the SCMC stacker from Fig. 4(e) and (f), suggested that the plane wave was oscillating in each resonant cavity with a symmetric distribution. The maximum power of a vertical incident plane wave at 520 nm was appeared at the center of each resonant cavity. The peak power values showed in the cavities of the core repeated periodicities were larger than that in the top cavity and the bottom cavity with fewer layers of distributed Bragg reflector. Similar phenomena about the oscillation of standing waves in each resonant cavity with an incident angle of 45° for the linearly *p*-polarized wave at 474 nm and for the linearly *s*-polarized wave at 469 nm, was observed in Fig. 5.

IV. Conclusion

To summarize, we designed a CMOS compatible SCMC band pass optical filter on a glass substrate based on SiN/SiO_2 materials, for the application in fluorescence detection such as FAM with an emission spectrum centered on 520 nm by a 488 nm laser source. The computations based on TMM calculation and 2D FDTD algorithm, revealed that the average transmittance value in the pass band region reduced almost linearly from 92.73% to 76.45% with the increasing of the number of resonant cavities in the SCMC stacker from 3 to 20. Reversely, the maximum optical density value in the block region improved linearly from -2.88 to -25.28 with the increment of the number of resonant cavities from 3 to 20. Therefore, to choose a design that with a high transmittance pass band and a high optical density to block the unwanted waves, a moderate number of the resonant cavities should be selected. The calculation of transmittance for a SCMC band pass optical filter *Air/(HL)^2 H2LH(LH)^{2}L [(HL)^{3}H2 LH (LH)^{3}L]^8(HL)^{2}H2LH (LH)^2/Glass* with $m = 10$ dependent on angle of incidence for linearly p/s polarized light, suggested that the center wavelength of the pass band blue-shifted from 520 nm to 474 nm (469 nm) with the increasing of incident angle from 0 to 45°. The range of the incident angle for enabling fluorescence emission at 520 nm passing through and laser excitation wave at 488 nm blocked well, should be under 18°. Thus, we concluded that a microlens array with suitable focus lengths together with micro-aperture of matched opening sizes that above the SCMC, were in necessary to integrate with the SCMC bandpass optical filter to direct the light to incident on its surface and to enable the

fluorescence emission passing through with a focus in the active regions of CMOS sensors with low crosstalk. Our calculation based on 2D FDTD simulation in wavelength scale, uncovered the propagation of incident waves at center wavelength through the SCMC band pass optical filter and showed the power oscillations in each resonant cavity in addition. The SiN/SiO_2 materials platform that can be deposited by both the PECVD and PVD technique and compatible with the CMOS semiconductor process, made it possible to be integrated with PIC, lab-on-chip, and CMOS sensors (or photo-detectors), to enable fast-response, high accuracy, and handheld point-of-care diagnosis protocol available in future.

REFERENCES

[1] R. R. Singh, D. Ho, A. Nilchi, R. Genov, and G. Gulak, "A hybrid thin-film/CMOS fluorescence contact imager," in *Proc. IEEE Int. Symp. Circuits Syst.*, 2009, pp. 2437–2440.

[2] A. Manickam et al., "A fully integrated CMOS fluorescence biochip for DNA and RNA testing," *IEEE J. Solid-State Circuit*, vol. 52, no. 11, pp. 2857–2870, Nov. 2017.

[3] A. Priye, C. S. Ball, and R. J. Meagher, "Colorimetric-luminance readout for quantitative analysis of fluorescence signals with a smartphone CMOS sensor," *Anal. Chem.*, vol. 90, no. 21, pp. 12385–12389, 2018.

[4] T. Gou et al., "Smartphone-based mobile digital PCR device for DNA quantitative analysis with high accuracy," *Biosensors Bioelectron.*, vol. 120, pp. 144–152, 2018.

[5] A. Hofmann, M. Meister, A. Rolapp, P. Reich, F. Scholz, and E. Schäfer, "Light absorption measurement with a CMOS biochip for quantitative immunoassay based point-of-care applications," *IEEE Trans. Biomed. Circuits Syst.*, vol. 15, no. 3, pp. 369–379, Jun. 2021.

[6] S.-H. Yun et al., "Cost-effective multiplex fluorescence detection system for PCR chip," *Sensors*, vol. 21, no. 21, 2021, Art. no. 6945.

[7] Y.-H. Shin et al., "Review—Recent progress in portable fluorescence sensors," *J. Electrochem. Soc.*, vol. 168, no. 1, 2021, Art. no. 017502.

[8] C. P. Chen et al., "Double-layer Fabry-Pérot filter interferometric modulator display," *J. Inf. Display*, vol. 14, no. 4, pp. 121–125, 2013.

[9] B. A. Belyaev, V. V. Tyurnev, and V. F. Shabanov, "Design of optical bandpass filters based on a two-material multilayer structure," *Opt. Lett.*, vol. 39, no. 12, pp. 3512–3515, 2014.

[10] B. A. Belyaev, V. V. Tyurnev, and V. F. Shabanov, "One-dimensional photonic crystal bandpass filters," *Doklady Phys.*, vol. 59, no. 2, pp. 73–78, 2014.

[11] B. A. Belyaev and V. V. Tyurnev, "Multilayer bandpass filter with extended lower and upper stop bands," *Opt. Lett.*, vol. 40, no. 18, pp. 4333–4335, 2015.

[12] M. Niraula, J. W. Yoon, and R. Magnusson, "Single-layer optical bandpass filter technology," *Opt. Lett.*, vol. 40, no. 21, pp. 5062–5065, 2015.

[13] C. P. Chen, Y. Li, Y. Su, G. He, J. Lu, and L. Qian, "Transmissive interferometric display with single-layer Fabry–Pérot filter," *J. Display Technol.*, vol. 11, no. 9, pp. 715–719, 2015.

[14] B. A. Belyaev and V. V. Tyurnev, "Design of bandpass filters composed of dielectric layers separated by gratings of strip conductors," *Opt. Lett.*, vol. 41, no. 3, pp. 536–539, 2016.

[15] Y. H. Ko, M. Niraula, and R. Magnusson, "Divergence-tolerant resonant bandpass filters," *Opt. Lett.*, vol. 41, no. 14, pp. 3305–3308, 2016.

[16] Y. H. Ko and R. Magnusson, "Flat-top bandpass filters enabled by cascaded resonant gratings," *Opt. Lett.*, vol. 41, no. 20, pp. 4704–4707, 2016.

[17] A. Melnyk et al., "Air gap resonant tunneling bandpass filter and polarizer," *Opt. Lett.*, vol. 41, no. 8, pp. 1845–1848, 2016.

[18] T. R. Harrison et al., "Widely tunable bandpass filter based on resonant optical tunneling," *Opt. Exp.*, vol. 27, no. 16, pp. 23633–23644, 2019.

[19] P. Baumeister, "Prediction of the bandwidth of an all-dielectric bandpass filter," *Appl. Opt.*, vol. 30, no. 28, pp. 4066–4068, 1991.

[20] H. A. Macleod, *Thin-Film Optical Filters*, 5th ed. Boca Raton, FL, USA: CRC Press, 2017.

[21] B. A. Belyaev and V. V. Tyurnev, "Diffraction of electromagnetic waves on a one-dimensional strip conductor grating located at the interface between dielectric media," *Russian Phys. J.*, vol. 58, no. 5, pp. 646–657, 2015.

[22] S. Robinson and R. Nakkeeran, "Investigation on two dimensional photonic crystal resonant cavity based bandpass filter," *Optik*, vol. 123, no. 5, pp. 451–457, 2012.

[23] Y. I. A. Al-Yasir et al., "A survey of differential-fed microstrip bandpass filters: Recent techniques and challenges," *Sensors*, vol. 20, no. 8, 2020, Art. no. 2356.

[24] N. H. T. Tran et al., "Fluorescence enhancement using bimetal surface plasmon-coupled emission from 5-carboxyfluorescein (FAM)," *Micromachines*, vol. 9, no. 9, 2018, Art. no. 460.

[25] X. Shi et al., "A novel bio-sensor based on DNA strand displacement," *Plos One*, vol. 9, no. 10, 2014, Art. no. e108856.

[26] U. S. Inan and R. A. Marshall, *Numerical Electromagnetics: The FDTD Method*. Cambridge, U.K.: Cambridge Univ. Press, 2011.

[27] R. Rumpf, "Design and optimization of nano-optical elements by coupling fabrication to optical behavior," Ph.D. dissertation, College Optics Photonics, Univ. Central Florida, Orlando, FL, USA, 2006.